High Open-Circuit Voltages: Evidence for a Sensitizer-Induced TiO2 Conduction Band Shift in Ru(II)-Dye Sensitized Solar Cells

ARTICLE *in* CHEMISTRY OF MATERIALS · NOVEMBER 2013

Impact Factor: 8.35 · DOI: 10.1021/cm401872q

CHEMISTRY OF MATERIALS

Article

pubs.acs.org/cm

High Open-Circuit Voltages: Evidence for a Sensitizer-Induced TiO_2 Conduction Band Shift in Ru(II)-Dye Sensitized Solar Cells

Thomas Moehl,[†] Hoi Nok Tsao,[†] Kuan-Lin Wu,[†,§] Hui-Chu Hsu,[§] Yun Chi,*[,§] Enrico Ronca,[‡] Filippo De Angelis,*[,‡] Mohammad K. Nazeeruddin,*[,†] and Michael Grätzel[†]

[†]Laboratory for Photonics and Interfaces, Institute of Chemical Sciences and Engineering, École Polytechnique Fédérale de Lausanne, Lausanne - 1015, Switzerland

[‡]Computational Laboratory for Hybrid/Organic Photovoltaics (CLHYO), CNR-ISTM, via Elce di Sotto 8, I-06123, Perugia, Italy

[§]Department of Chemistry and Low Carbon Energy Research Center, National Tsing Hua University, Hsinchu 30013, Taiwan

Supporting Information

ABSTRACT: Dye-sensitized solar cells (DSC) represent a valuable, efficient, and low-cost alternative to conventional semiconductor photovoltaic devices. A deeper understanding of the interactions at the dye/semiconductor heterointerface is fundamental for future progress in DSC technology. Here we present an interesting heteroleptic ruthenium(II) sensitizer that shifts the conduction band of TiO_2 by 80 mV resulting in high open circuit potential for improved device efficiency.

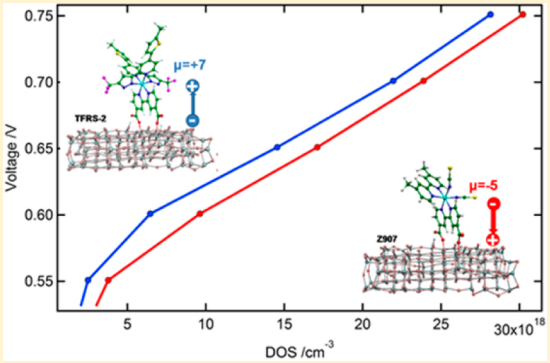

KEYWORDS: *dye sensitized solar cell, dye dipole, impedance spectroscopy, DFT, open circuit voltage*

INTRODUCTION

Since the first proof of concept by O'Regan and Grätzel 20 years ago considerable attention and extensive research efforts have been devoted to dye sensitized solar cells (DSC)[1] as a valuable and low-cost alternative to silicon and other inorganic semiconductor-based photovoltaic devices. In DSC, a dye adsorbed at the surface of a wide band gap semiconductor (usually nanostructured TiO_2) absorbs light and injects an electron into the semiconductor conduction band, followed by dye regeneration by a liquid redox electrolyte (usually based on the I^-/I_3^- redox couple) or a solid hole conductor. Up to now, Ru(II)-polypyridyl sensitizers endowed with carboxy-substituted bipyridine ligands as anchoring groups have shown the highest DSC performances with solar energy-to-electricity conversion efficiencies exceeding 11%,[2−14] only superseded recently by Yella et al.[15]

Higher photovoltaic efficiencies are needed for widespread applications of DSC devices. The overall conversion efficiency (η) of a DSC is determined by the product of the short circuit current density (J_{SC}), the open circuit potential (V_{OC}), and the fill factor (FF) of the cell, normalized to the intensity of the incident light (I_s), namely, $\eta = J_{SC} \times V_{OC} \times FF/I_s$. A straightforward and successful strategy which has been employed to obtain high DSC efficiencies is to engineer new Ru(II) heteroleptic dyes with improved light-harvesting capability. This has been achieved either by red-shifting the dye absorption spectrum or by increasing the molar extinction coefficient of the electronic transitions in the visible to near-IR spectral portion, thus leading to enhanced J_{SC}.[2−14] On the contrary, the V_{OC} is dictated by the difference between the semiconductor quasi-Fermi level under illumination and the electrolyte redox potential and only indirectly dependent on the dye. One known way to tune the conduction band of the mesoporous semiconductor oxide and, therefore, the DSC V_{OC}, by the dye is related to the number of protons carried by the anchoring groups of the dyes. Most common examples of this effect are the isostructural ruthenium dyes N3 (four times protonated) and N719 (two times protonated). Nazeeruddin et al. also investigated the mono- and triprotonated form of N3 leading to a voltage difference between N3 and its fully deprotonated form of 300 mV.[16] Apart from the change of the conduction band by the acidity of the dyes anchoring groups, engineering of new dyes endowed with a predictably high V_{OC} has been so far scarcely explored.[17−20] On the other hand various investigations have, however, found that the presence of certain groups attached in critical positions of the dye or that insufficient dye regeneration at higher forward bias might lead to increased recombination and ultimately lead to a reduced V_{OC} of the related DSC devices.[21−32]

Received: May 22, 2013
Revised: November 1, 2013
Published: November 1, 2013

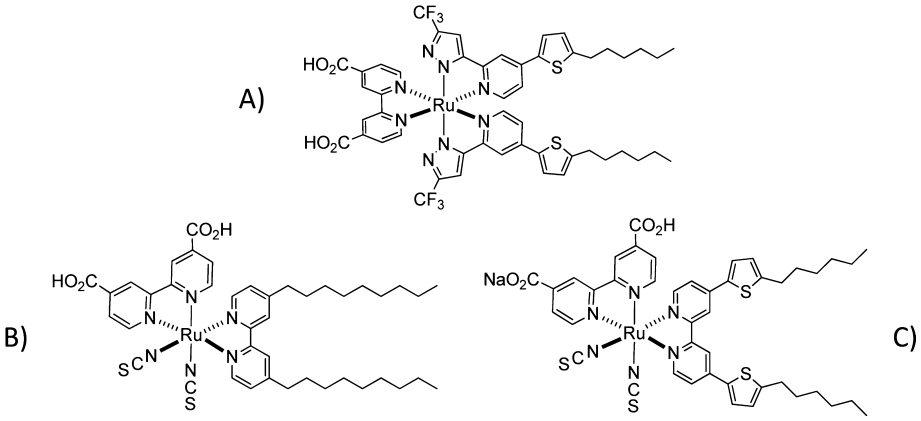

Figure 1. Geometrical structures of the dyes: (A) TFRS-2, (B) Z907, and (C) C101.

Interestingly, experiments also showed that the V_{OC} delivered by DSCs employing Ru(II) heteroleptic dyes can be significantly lower compared to that observed using the prototype homoleptic N719 dye.[25] A homoleptic dye like N719 can bind by three carboxylate groups to the TiO_2 surface.[33] This leads to an increased electron donating effect by the additional binding group and a possible closer packing of the dye at the surface, reducing dark current and therefore recombination. A similarly high V_{OC} (ca. 800 mV) was reported for the homoleptic Ru(II) YE-05 dye, which suggested a correlation between the dye adsorption mode and the DSCs V_{OC}.[33−35] Another origin for the change in *V*oc can be the electrostatic potential, related to the charge distribution and the dipole moment, of the dye itself.[36] For positive dipoles, i.e., with the negative pole near the TiO_2 surface, an upward shift of the conduction band can be achieved,[36−38] while leaving the recombination behavior largely unchanged. Very recently, a series of new neutral thiocyanate-free sensitizers incorporating two 2-(4-(5-hexylthiophene))-pyridyl 4-(trifluoromethyl)-pyrazolate ancillaries and one 4,4′-dicarboxylic acid 2,2-bipyridyl ligand, coded TFRS-2, Figure 1, have shown to provide V_{OC} values of 810−830 mV in optimized DSCs.[39,40] This observation is remarkable and represents the first case in which high V_{OC}, comparable to that of N719,[39] was obtained with a dye bearing a single 4,4′-dicarboxylic ligand.

A deeper understanding of the dye/semiconductor heterointerface is fundamental for further progress in DSC technology. Here we wish to enlighten the reason underlying the high open circuit voltage of DSCs based on the heteroleptic TFRS-2 dye. We thus undertake a comparative study combining experimental and computational investigations on DSCs based on TFRS-2 and comparable highly efficient heteroleptic ruthenium based dyes, i.e., C101 and Z907. The chosen dyes allow us to investigate the effect of the dye ancillary ligands, maintaining the same single bipyridine anchoring.

EXPERIMENTAL SECTION

Fabrication of Devices. The DSCs in this investigation were composed of a photoanode on FTO glass (NSG-10) with a 5 μm thin transparent nanoporous TiO_2 and 4 μm thick scattering layer superimposed. The active area of the TiO_2 film was 0.16 cm^2. A platinized FTO glass was used as the counter electrode. The TiO_2 film was stained with the dye by immersing it for 10 h in a 0.1 mM dye solution in *tert*-butanol/acetonitrile mixture (1:1 v/v). TFRS-2,[32] C101, and Z907[13] dyes were available from our previous studies. The electrolyte used (Z946) consists of 3-methoxypropionitrile with 1.0 M DMII, 0.15 M I_2, and 0.5 M NBB (*N*-butylbenzimidazole) as well as 0.1 M guanidinium thiocyanate. A similar run was performed with a 13 μm thin transparent mesoporous TiO_2 film using a different electrolyte (A6141) consisted of 0.6 M butylmethylimidazolium iodide (BMII), 0.03 M I_2, 0.10 M guanidinium thiocyanate, and 0.50 M *tert*-butylpyridine in valeronitrile and acetonitrile (15:85 v/v).

A more detailed description of the making of such devices and the involved steps can be found in the publications from Ito et al.[5,41]

Photovoltaic Characterization. Current−voltage characteristics were recorded by applying an external potential bias to the cell while recording the generated photocurrent with a Keithley model 2400 digital source meter. The light source was a 450 W xenon lamp (Oriel) equipped with a Schott K113 Tempax sunlight filter (Praezisions Glas & Optik GmbH) in order to match the emission spectrum of the lamp to the AM1.5G standard.

Transient measurements: A diode array (Lumiled, Model LXHL-NWE8 White Star) was used to generate a white light bias. A perturbation excitation was produced by a red-light pulsed diode (LXHLND98 Redstar, 0.2 s square pulse width, 100 ns rise and fall time) controlled by a fast solid-state switch. A Keithley sourcemeter monitored the voltage and current dynamics. The voltage decay measurements were conducted at V_{OC} with varying white light bias intensities. The photocurrent transient decay measurements, J_{SC}, were conducted to determine the differential charge density and extract the capacitance at each light intensity.[42]

Impedance measurements: The impedance measurements have been performed with a BioLogic SP300 potentiostat. A sinusoidal potential perturbation (amplitude of 15 mV) was applied over a frequency range of 7 MHz−0.1 Hz at constant potential bias. The bias potential was varied between 0 mV and V_{OC} with about 50 mV steps. The impedance spectra were fitted with the ZView software (Scribner Associates) using the transmission model line.[43]

RESULTS AND DISCUSSION

We fabricated DSCs employing the three dyes under identical conditions, employing two different iodine-based electrolytes. Afterward we (i) measured the related IV curves; (ii) performed charge extraction and V_{OC} decay measurements as a function of light intensity; (iii) performed EIS measurements in the dark and under illumination; and (iv) measured the dye coverage. On the computational side, we simulated the dyes' (TFRS-2 vs Z907) adsorption mode on TiO_2, calculated the effect of dye adsorption on the position of the TiO_2 conduction band, and rationalized the observed trend in terms of electrostatic potential and dye dipole moment.

Figure 2 presents the current−voltage curves in the dark and for simulated full sunlight (intensity 100 mW cm^{-2}) for the devices employing the Z946 electrolyte. Table 1 shows the photovoltaic characteristics of these DSCs along with the

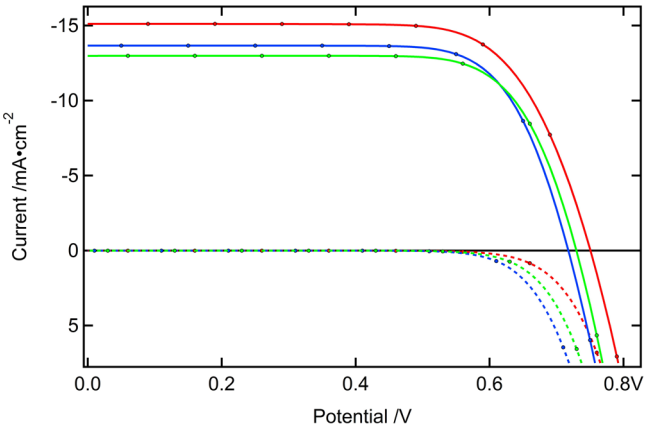

Figure 2. $I-V$ curves measured for DSCs based on TFRS-2 (red), C101 (blue), and Z907 (green) dyes under 1 sun AM1.5 solar irradiation (solid line) and dark conditions (dashed line).

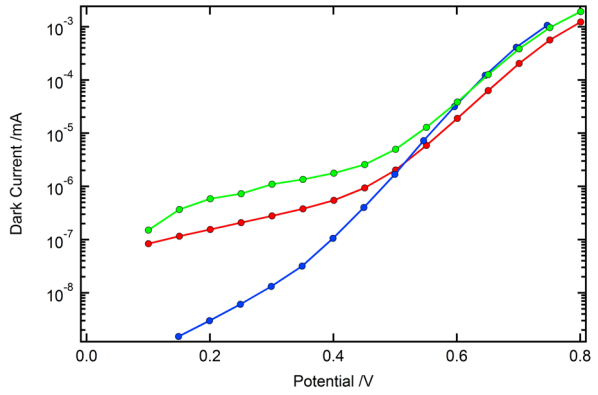

Figure 3. Dark current from the EIS measurements for DSCs based on TFRS-2 (red), C101 (blue), and Z907 (green) dyes plotted in logarithmic scale.

measured dye loading for each dye. Under the employed conditions TFSR-2 shows the highest performance, due to a higher J_{SC} and V_{OC} compared to C101 and Z907. It is very interesting to notice that the three dyes exhibit a similar dye loading, which does not correlate with the V_{OC}, so this cannot be the reason for the higher V_{OC} observed for TFRS-2.

In Figure 3 the dark currents of three typical DSCs during the EIS measurement are presented. One can observe that the change of the dye leads to changes in the dark current. This can be either due to the change in the E_{CB} of the TiO_2 or to the change in the recombination behavior at the interface metal oxide/electrolyte or to a combination of both factors.

The origin of the different V_{OC} was in the following step investigated by charge extraction and V_{OC} decay measurements as a function of light intensity (transient measurements).

The results from the transient measurements (performed after Duffy et al.[42]) are presented in Figure 4. The capacitance of the mesoporous TiO_2 determined from the charge extraction measurements shows a nearly constant shift of ~28 (20) mV between TFSR-2 and C101 (Z907). Also the electron lifetime in relation to the chemical capacitance (indirect measure of the E_F) differs. The longest lifetime is measured for TFSR-2 followed by Z907 and C101. The difference in electron lifetime itself is small but resulting also in minor changes in the final V_{OC} of the devices. A rough estimation over the diode equation ($\Delta V_{OC} = (k_B T/q)(\ln(\tau_1/\tau_2)$ with k_B as Boltzmann constant, T as temperature, and q as elemental charge) leads to a change of the V_{OC} between TFSR-2 and C101 of about 18 mV (with Z907 of 10 mV). The differences in V_{OC} observed from Table 1 are 44 mV between TFSR-2 and C101 (25 mV for Z907) which matches well with the expected differences from the sum of the conduction band shift and electron lifetime (46 mV and 30 mV) from the transient measurements.

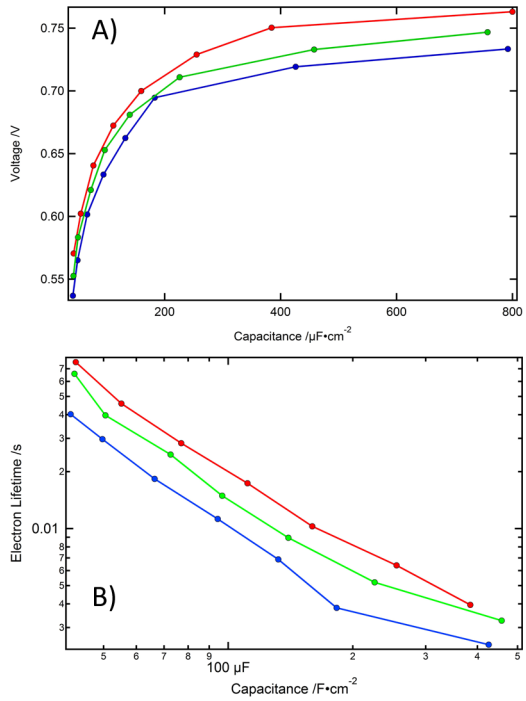

Figure 4. (A) Capacitance of the TiO_2 in DSCs sensitized by TFRS-2 (red), C101 (blue), and Z907 (green). (B) Electron lifetime of DSCs sensitized with TFRS-2 (red), C101 (blue), and Z907 (green).

Electrochemical impedance spectroscopy (EIS) measurements could confirm the results of the transient measurements (Figure 5). All parameters of the EIS measurements were extracted by fitting with the transmission line model.[43] In Figure 5A, we present the most relevant results of the EIS fitting: the transport resistance for electrons inside the TiO_2, the recombination resistance accounting for the recombinative

Table 1. Photovoltaic Parameters of DSC Based on the Three Dyes Employing the Z946 Electrolyte: 3-Methoxypropionitrile with 1.0 M DMII, 0.15 M I_2, and 0.5 M NBB as well as 0.1 M Guanidinium Thiocyanate[a]

dye	dye loading (10^{-10} mol/cm^2)	J_{SC} (mA/cm^2)	V_{OC} (mV)	FF	η (%)
TFRS-2	0.95	14.8 ± 0.3	754 ± 5	0.73 ± 0.02	8.0 ± 0.2
Z907	0.91	12.9 ± 0.2	729 ± 3	0.74 ± 0.02	6.9 ± 0.2
C101	1.04	13.4 ± 0.3	710 ± 5	0.75 ± 0.02	7.1 ± 0.2

[a]The $I-V$ data represents the average out of two devices each.

dx.doi.org/10.1021/cm401872q | Chem. Mater. 2013, 25, 4497−4502

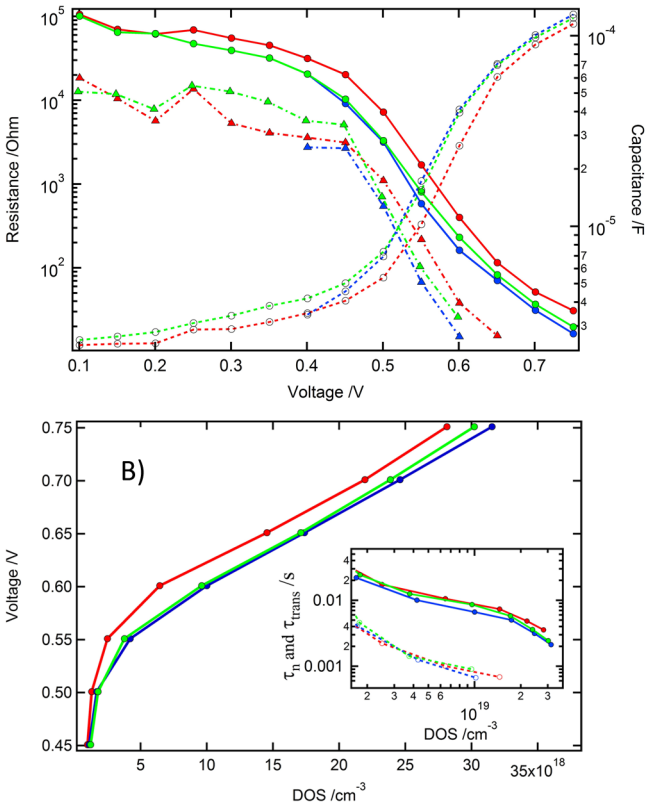

Figure 5. EIS under illumination: (A) Transport resistance of the TiO_2 (triangle), recombination resistance between the TiO_2 and the electrolyte (filled circles), and the chemical capacitance of the TiO_2 (empty circles) under illumination for TFRS-2 (red), C101 (blue), and Z907 (green) plotted against applied potential. (B) Applied potential vs DOS from the EIS measurements. Inset shows the electron transport (dotted) and lifetime (solid) vs DOS for TFRS-2 (red), C101 (blue), and Z907 (green).

charge transfer of electrons from the TiO_2 to the electrolyte, and the chemical capacitance of the TiO_2. As seen in Figure 5B, the shift in E_{CB} is very similar to the results of charge extraction measurements (~22 mV between TFRS-2 and C101 (17 mV for Z907)). The inset in Figure 5B shows the electron lifetimes plotted against the DOS of the TiO_2 and the same tendencies like in the case of the transient measurement (see Figure 4). The estimation for the change in V_{OC} from the different electron lifetimes gives in the EIS measurement a change of 10 mV between the TFSR-2 and C101 (7 mV for the Z907). With the determined change in conduction band position one yields 32 mV for C101 and 24 mV for Z907 based devices as expected change in V_{OC} compared to TFSR-2.

The same investigations were also conducted with the A6141 electrolyte leading to similar results (see Supporting Information, Figure S1, S2 for the results of the transient measurements and S3, S4 and S5 for the EIS results). Higher V_{OC} values were obtained with this electrolyte but the differences in V_{OC} among the three dyes were still observed, with V_{OC} values of 855, 797, and 814 mV for TFRS-2, C101 and Z907, respectively.

In case of a more volatile solvent paired with a lower concentration of the iodine and iodide in the electrolyte used the differences in conduction band positions are even more pronounced (A6141 vs Z946). An explanation for this observation is probably the fact that in the case of the higher concentration of the redox system (Z946) a higher screening of the surface-adsorbed species electrostatic potential might reduce the influence of the dye dipole.

The plot of the electron lifetime and transport time vs DOS (calculated from the EIS results, see Supporting Information Figure S4 and S5) shows that the transport time differs only slightly with different dyes in the devices (at the same DOS) but the recombination behavior is influenced (see also Supporting Information Figure S2 for the transient measurements). So both, transient and EIS measurements revealed that the dyes impose next to a change in E_{CB} a different recombination behavior. EIS measurements also proved that the transport properties are not changing with a different dye at the surface of the TiO_2.

To gain insight into the origin of the TiO_2 E_{CB} shift by different dyes, we performed DFT calculations for the TFRS-2 and Z907 dyes adsorbed onto an anatase $(TiO_2)_{82}$ slab[26] exposing the majority (101) surfaces, of sufficiently large dimension to avoid spurious interactions between the dye anchoring groups and the cluster border.

As anticipated, the two dyes carrying the same bipyridine anchoring ligand show a similar adsorption mode (see Figure 6), characterized by two dissociative monodentate carboxylic

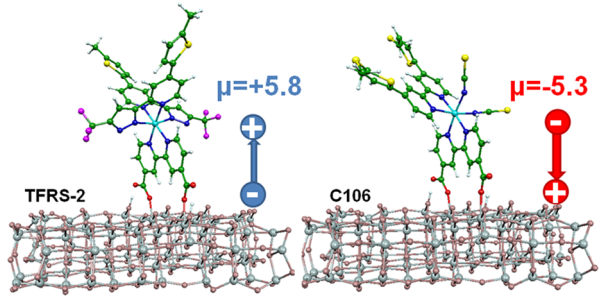

Figure 6. Optimized geometries of TFRS-2 (left) and Z907 (right) along with the calculated dipole moments of the neutral dyes at their adsorption geometries. Alkyl chains have been replaced by methyl groups.

groups. When a dye binds to a semiconductor surface, two effects might be at work: (a) the electrostatic (EL) effect, due to the dye charge distribution, including the dye dipole moment, and (b) the effect of the charge transfer (CT) between the dye and the semiconductor, which may accompany the dye−semiconductor bond formation. Using a recently developed computational approach,[29] we evaluated both the EL potential on the TiO_2 surface and the CT term (dye → semiconductor) for the two dyes. While the CT is large but nearly constant for TFRS-2 and Z907 (0.794 vs 0.790 e, respectively), the EL potential is sizably higher for TFRS-2 than for Z907 (−3.651 vs −3.436 eV, respectively). Since for charged species, such as the dyes with dissociated carboxylic groups, the dipole moment is ill defined (conversely to the EL potential), here we resort to the dye neutral species at their surface adsorbed geometries, obtained by protonating the two carboxylic groups, to evaluate the contribution of the dye dipole to the EL potential (which for neutral species is the only contribution, apart from higher multipoles, usually negligible).

The different dipole (see Figure 6) is expected to substantially influence the TiO_2 E_{CB}, leading to an energy down-shift for Z907 compared to TFRS-2. We therefore calculated the density of unoccupied states in the TiO_2

dx.doi.org/10.1021/cm401872q | Chem. Mater. 2013, 25, 4497−4502

conduction band region. The results are reported in Figure 7, which shows a ca. 20 meV energy upshift over a wide energy

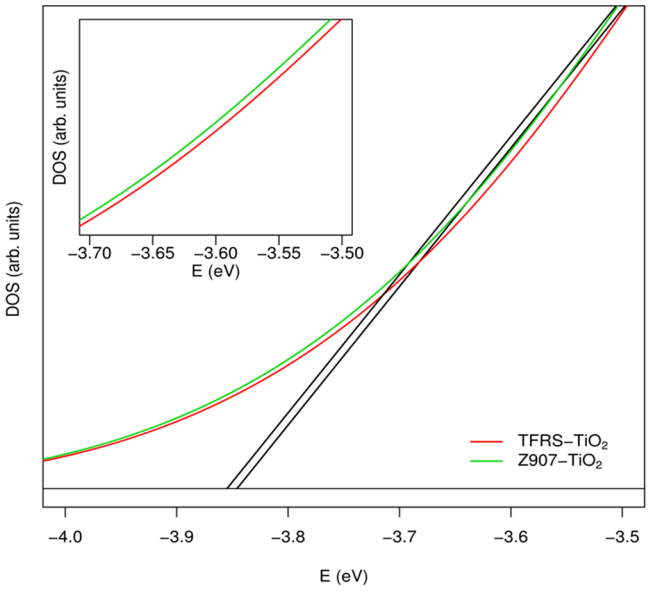

Figure 7. Density of unoccupied states in the TiO_2 conduction band region for TFRS-2 (red) and Z907 (green). The black lines represent the intercept with the energy axis, from which the E_{cb} value is extracted.

range for TFRS-2, compared to Z907, in line with the dipole effect discussed above and in agreement with the picture extracted from the device characterization.

The most noticeable difference between the two systems is indeed the different magnitude and orientation of the dye dipole moment component normal to the TiO_2 surface (see Figure 6), which is possibly related to the E_{CB} shift. As found previously,[30] the negative charge localized on the thiocyanate ligands prevails over that of the carboxylic groups in determining the negative dipole (−5 D) of Z907 and of related heteroleptic dyes, with location of the positive pole close to the TiO_2 surface. For TFRS-2, on the other hand, a positive dipole is calculated (+7 D), due to symmetric and delocalized nature of the charge density, which is shared between the metal and the anionic ligands. Following the analysis of ref 38, we can also evaluate the expected E_{CB} shift related to the calculated dipole moment difference (12 D). At the dye coverage of our simulations (ca. 1 dye molecule over 4 nm^2 of TiO_2 surface), a shift of 18 meV/D can be expected assuming a dielectric constant of 5 for the interface monolayer.[31] Thus an overall ∼200 meV E_{CB} shift could be expected for a 12 D dipole at the considered coverage against the ∼20 meV which we calculate here. The difference between the expected and calculated values can possibly be related to the fact that our simulations are performed in acetonitrile solution, which effectively screens the EL dye/semiconductor interaction by virtue of the high dielectric constant. The presence of ionic additives in the electrolyte may also explain the observed reduction of the measured E_{CB} shift from its expectedly higher value.

CONCLUSIONS

We have demonstrated that the structure and the resulting dipole moment of the TFRS-2 dye can effectively be exploited to tune the TiO_2 conduction band energy and therefore the DSCs open-circuit voltage. Both theory and experiments show a conduction band upward shift in TFRS-2 sensitized TiO_2 contributing to the high V_{OC} of the DSCs based on this dye. Our study provides the interpretative basis for future development of more efficient solar cells sensitizers.

ASSOCIATED CONTENT

Supporting Information

Additional figures. This material is available free of charge via the Internet at http://pubs.acs.org.

AUTHOR INFORMATION

Notes

The authors declare no competing financial interest.

ACKNOWLEDGMENTS

The authors are grateful for the FP7-NMP-2009 project SANS (246124) and the ECR advanced Grant Agreement no. 247404 under the CE-Mesolight project funded by the European community's seventh FWP for the for financial support. E.R. and F.D.A. thank CNR-EFOR for a grant. M.K.N. thanks the World Class University programmes (Photovoltaic Materials, Department of Material Chemistry, Korea University), funded by the Ministry of Education, Science and Technology through the National Research Foundation of Korea (R31-2008-000-10035-0).

REFERENCES

(1) O'Regan, B.; Gratzel, M. *Nature* **1991**, *353*, 737−740.
(2) Nazeeruddin, M. K.; Kay, A.; Rodicio, I.; Humphry-Baker, R.; Muller, E.; Liska, P.; Vlachopoulos, N.; Gratzel, M. *J. Am. Chem. Soc.* **1993**, *115*, 6382−6390.
(3) Nazeeruddin, M. K.; De Angelis, F.; Fantacci, S.; Selloni, A.; Viscardi, G.; Liska, P.; Ito, S.; Bessho, T.; Gratzel, M. *J. Am. Chem. Soc.* **2005**, *127*, 16835−16847.
(4) Mishra, A.; Pootrakulchote, N.; Fischer, M. K. R.; Klein, C.; Nazeeruddin, M. K.; Zakeeruddin, S. M.; Bauerle, P.; Gratzel, M. *Chem. Commun.* **2009**, 7146−7148.
(5) Ito, S.; Zakeeruddin, S. M.; Humphry-Baker, R.; Liska, P.; Charvet, R.; Comte, P.; Nazeeruddin, M. K.; Pechy, P.; Takata, M.; Miura, H.; Uchida, S.; Gratzel, M. *Adv. Mater.* **2006**, *18*, 1202.
(6) Ito, S.; Miura, H.; Uchida, S.; Takata, M.; Sumioka, K.; Liska, P.; Comte, P.; Pechy, P.; Graetzel, M. *Chem. Commun.* **2008**, 5194−5196.
(7) Zhang, G. L.; Bala, H.; Cheng, Y. M.; Shi, D.; Lv, X. J.; Yu, Q. J.; Wang, P. *Chem. Commun.* **2009**, 2198−2200.
(8) Yum, J. H.; Walter, P.; Huber, S.; Rentsch, D.; Geiger, T.; Nuesch, F.; De Angelis, F.; Gratzel, M.; Nazeeruddin, M. K. *J. Am. Chem. Soc.* **2007**, *129*, 10320−10325.
(9) Liu, Y.; Hagfeldt, A.; Xiao, X. R.; Lindquist, S. E. *Sol. Energy Mater. Sol. Cells* **1998**, *55*, 267−281.
(10) Diguna, L. J.; Shen, Q.; Sato, A.; Katayama, K.; Sawada, T.; Toyoda, T. *Mater. Sci. Eng. C* **2007**, *27*, 1514−1520.
(11) Jung, Y. S.; Yoo, B.; Lim, M. K.; Lee, S. Y.; Kim, K. J. *Electrochim. Acta* **2009**, *54*, 6286−6291.
(12) Mikoshiba, S.; Murai, S.; Sumino, H.; Kado, T.; Kosugi, D.; Hayase, S. *Curr. Appl. Phys.* **2005**, *5*, 152−158.
(13) Kroeze, J. E.; Hirata, N.; Koops, S.; Nazeeruddin, M. K.; Schmidt-Mende, L.; Gratzel, M.; Durrant, J. R. *J. Am. Chem. Soc.* **2006**, *128*, 16376−16383.
(14) Law, C. H.; Pathirana, S. C.; Li, X. O.; Anderson, A. Y.; Barnes, P. R. F.; Listorti, A.; Ghaddar, T. H.; O'Regan, B. C. *Adv. Mater.* **2010**, *22*, 4505−4509.
(15) Yella, A.; Lee, H. W.; Tsao, H. N.; Yi, C. Y.; Chandiran, A. K.; Nazeeruddin, M. K.; Diau, E. W. G.; Yeh, C. Y.; Zakeeruddin, S. M.; Gratzel, M. *Science* **2011**, *334*, 629−634.

(16) Nazeeruddin, M. K.; Humphry-Baker, R.; Liska, P.; Gratzel, M. *J. Phys. Chem. B* **2003**, *107*, 8981−8987.
(17) Duncan, W. R.; Stier, W. M.; Prezhdo, O. V. *J. Am. Chem. Soc.* **2005**, *127*, 7941−7951.
(18) Duncan, W. R.; Craig, C. F.; Prezhdo, O. V. *J. Am. Chem. Soc.* **2007**, *129*, 8528−8543.
(19) Fischer, S. A.; Duncan, W. R.; Prezhdo, O. V. *J. Am. Chem. Soc.* **2009**, *131*, 15483−15491.
(20) Duncan, W. R.; Prezhdo, O. V. *J. Am. Chem. Soc.* **2008**, *130*, 9756−9762.
(21) Rocca, D.; Gebauer, R.; De Angelis, F.; Nazeeruddin, M. K.; Baroni, S. *Chem. Phys. Lett.* **2009**, *475*, 49−53.
(22) Walker, B.; Saitta, A. M.; Gebauer, R.; Baroni, S. *Phys. Rev. Lett.* **2006**, *96*, 113001.
(23) Walker, B.; Gebauer, R. *J. Chem. Phys.* **2007**, *127*, 164106.
(24) Vittadini, A.; Selloni, A.; Rotzinger, F. P.; Gratzel, M. *Phys. Rev. Lett.* **1998**, *81*, 2954−2957.
(25) Car, R.; Parrinello, M. *Phys. Rev. Lett.* **1985**, *55*, 2471−2474.
(26) O'Regan, B. C.; Walley, K.; Juozapavicius, M.; Anderson, A.; Matar, F.; Ghaddar, T.; Zakeeruddin, S. M.; Klein, C.; Durrant, J. R. *J. Am. Chem. Soc.* **2009**, *131*, 3541−3548.
(27) Listorti, A.; Durrant, J. R.; O'Regan, B. *Chem. Mater.* **2011**, *23*, 3381−3399.
(28) Barnes, P. R. F.; Anderson, A. Y.; Juozapavicius, M.; Liu, L.; Li, X.; Palomares, E.; Forneli, A.; O'Regan, B. C. *Phys. Chem. Chem. Phys.* **2011**, *13*, 3547.
(29) Li, F.; Jennings, J. R.; Wang, Q. *ACS Nano* **2013**, *7*, 8233−8242.
(30) Brown, D. G.; Sanguantrakun, N.; Schulze, B.; Schubert, U. S.; Berlinguette, C. P. *J. Am. Chem. Soc.* **2012**, *134*, 12354−12357.
(31) Miettunen, K.; Barnes, P. R. F.; Li, X.; Law, C.; O'Regan, B. C. *J. Electroanal. Chem.* **2012**, *677*−*680*, 41−49.
(32) Wu, K.-L.; Li, C.-H.; Chi, Y.; Clifford, J. N.; Cabau, L.; Palomares, E.; Cheng, Y.-M.; Pan, H.-A.; Chou, P.-T. *J. Am. Chem. Soc.* **2012**, *134*, 7488−7496.
(33) De Angelis, F.; Fantacci, S.; Selloni, A.; Nazeeruddin, M. K.; Gratzel, M. *J. Phys. Chem. C* **2010**, *114*, 6054−6061.
(34) Schiffmann, F.; VandeVondele, J.; Hutter, J.; Wirz, R.; Urakawa, A.; Baiker, A. *J. Phys. Chem. C* **2010**, *114*, 8398−8404.
(35) Sekar, N.; Gehlot, V. *Resonance* **2010**, *15*, 819−831.
(36) Ronca, E.; Pastore, M.; Belpassi, L.; Tarantelli, F.; De Angelis, F. *Energy Environ. Sci.* **2013**, *6*, 183−193.
(37) De Angelis, F.; Fantacci, S.; Selloni, A.; Gratzel, M.; Nazeeruddin, M. K. *Nano Lett.* **2007**, *7*, 3189−3195.
(38) Cahen, D.; Ruhle, S.; Greenshtein, M.; Chen, S. G.; Merson, A.; Pizem, H.; Sukenik, C. S.; Zaban, A. *J. Phys. Chem. B* **2005**, *109*, 18907−18913.
(39) Wu, K.-L.; Hsu, H.-C.; Chen, K.; Chi, Y.; Chung, M.-W.; Liu, W.-H.; Chou, P.-T. *Chem. Commun.* **2010**, *46*, 5124.
(40) Wu, K.-L.; Ku, W.-P.; Clifford, J. N.; Palomares, E.; Ho, S.-T.; Chi, Y.; Liu, S.-H.; Chou, P.-T.; Nazeeruddin, M. K.; Gratzel, M. *Energy Environ. Sci.* **2013**, *6*, 859−870.
(41) Ito, S.; Murakami, T. N.; Comte, P.; Liska, P.; Gratzel, C.; Nazeeruddin, M. K.; Gratzel, M. *Thin Solid Films* **2008**, *516*, 4613−4619.
(42) Duffy, N. W.; Peter, L. M.; Rajapakse, R. M. G.; Wijayantha, K. G. U. *Electrochem. Commun.* **2000**, *2*, 658−662.
(43) Fabregat-Santiago, F.; Bisquert, J.; Garcia-Belmonte, G.; Boschloo, G.; Hagfeldt, A. *Sol. Energy Mater. Sol. Cells* **2005**, *87*, 117−131.